

High-precision broadband linear polarimetry of early-type binaries IV. The DH Cephei binary system in the open cluster of NGC 7380^{*}

Yasir Abdul Qadir¹, Andrei V. Berdyugin¹, Vilppu Piirola¹,
Takeshi Sakanoi², and Masato Kagitani²

¹ Department of Physics and Astronomy, FI-20014 University of Turku, Finland
e-mail: yasir.abdulqadir@utu.fi

² Graduate School of Sciences, Tohoku University, Aoba-ku, 980-8578 Sendai, Japan

Received XX / Accepted XX

ABSTRACT

Aims. DH Cephei is a well-known massive O+O-type binary system on the northern sky, situated at the center of young open cluster NGC 7380. Our high-precision multi-band polarimetry clearly reveals that variations of linear polarization in this system are synchronous with the phase of the orbital period. We used the observed variations of Stokes parameters q and u to derive the orbital inclination i , orientation Ω , and the direction of rotation. Moreover, in order to obtain a rough estimation of the interstellar polarization in the vicinity of DH Cep, we observed polarization arising from the neighboring stars in the cluster.

Methods. We used the Dipol-2 polarimeter in combination with the remotely controlled 60 cm Tohoku T60 telescope to obtain linear polarization measurements of DH Cep in the B , V , and R passbands at the accuracy level of $\sim 0.003\%$. To obtain an estimation of interstellar polarization of DH Cep, we observed more than a dozen field stars identified as members of NGC 7380 and in the close proximity to DH Cep. A Lomb-Scargle period search was applied to the acquired polarization data to reveal the dominating frequency in polarization variations. We used a standard analytical method based on a two-harmonics Fourier fit to derive the inclination, orientation, and the direction of rotation of the binary orbit.

Results. The variations of Stokes parameters in all three B , V , and R passbands clearly suggest an unambiguous periodic signal at 1.055 d with an amplitude of variations of $\sim 0.2\%$, which corresponds to half of the known orbital period of 2.11 d. This type of polarization variability is expected for a binary system with light-scattering material distributed symmetrically with respect to the orbital plane. In addition to the regular polarization variability, there is a nonperiodic component, which is strongest in the B passband. In the V passband, we obtained our most reliable values for the orbital inclination $i = 46^\circ + 11^\circ / -46^\circ$ and an orientation of the orbit on the sky of $\Omega = 105^\circ \pm 55^\circ$, with 1σ confidence intervals. Using our best estimate of i and the polarimetric amplitude in the V passband, we estimated that the mass loss from the system is $\sim 3.4 \times 10^{-7} M_\odot \text{ yr}^{-1}$. The direction of the binary system rotation on the plane of the sky is clockwise. Our polarimetric observations of neighboring stars of DH Cep in NGC 7380 reveal that the polarization of the cluster stars is most likely due to aligned interstellar dust in the foreground.

Key words. polarization – techniques: polarimetric – instrumentation: polarimeters – stars: individual: DH Cephei – binaries (including multiple): close – binaries: non-eclipsing

1. Introduction

DH Cephei (DH Cep, or HD 215835) is a close binary system that consists of two O-type stars. It is the second-brightest member of the young open cluster NGC 7380 (Underhill 1969) and is located in the Perseus arm of the Galaxy at a distance of ~ 2.9 kpc (Gaia Collaboration et al. 2021). A number of photometric data analyses have been carried out over recent years, all of them suggesting that DH Cep is an elliptical variable with no signatures of eclipses (Moffat (1971); Wu & Eaton (1981); Lines et al. (1986)).

The first spectroscopic studies of this binary star system were carried out in 1949, where DH Cep was found to be a double-lined spectroscopic binary with a circular orbit and an orbital period of ~ 2.11 d (Pearce 1949). Lines et al. (1986) used their photometric observations to show that the photometric minima

are separated by half an orbital period, reconfirming the orbital period of 2.11 d. The latest photometric study of DH Cep by Lata et al. (2016)) also determined an orbital period of ~ 2.11 d.

A detailed study of the DH Cep system was conducted by Penny et al. (1997). These authors employed a Doppler tomography method and the UV spectra obtained with the International Ultraviolet Explorer (IUE) and identified the spectral type of the primary and secondary as O6V(O5 – O6.5) and O7V(O6.5 – O7.5), with the masses of $39 - 50 M_\odot$ and $35 - 45 M_\odot$, respectively. Penny et al. (1997) derived an upper limit on the inclination of $i < 43^\circ$ based on the combined absolute visual magnitude from the position on the Hertzsprung–Russell (HR) diagram. They also derived a lower limit of $i > 39^\circ$ and showed that below this value, the implied spectroscopic masses would become much larger than the evolutionary ones.

Moreover, being a hot and massive binary system, DH Cep is of particular interest to the field of high-energy astrophysics. The observations of this binary made in X-rays by Bhatt et al. (2010) determined $\log(L_X/L_{\text{bol}}) = -6.7$ in the 0.3 – 7.5 keV energy band. This latter study also suggested the presence of

^{*} The polarization data for DH Cep are only available in electronic form at the CDS via anonymous ftp to cdsarc.cds.unistra.fr (130.79.128.5) or via <https://cdsarc.cds.unistra.fr/cgi-bin/qcat?J/A+A/>

colliding winds and the presence of both a cool (< 1 keV) and a hot (> 1.89 keV) component, which are possibly associated with the instabilities in the radiation-driven wind shocks.

As DH Cep is a luminous object across different parts of the spectrum and is situated in a well-known open cluster, it is a relatively well-studied object of the northern sky. However, to date, there has only been one broadband polarimetric study of this binary system that probed a possible phase dependence of DH Cep linear polarization. The results of this study were reported by Corcoran (1991), who suggested the existence of a substantial aspherical envelope of ionized material around at least one of the binary stars, but failed to detect a phase dependence of the observed polarization variability. The main obstacle preventing a firm detection of phase-dependent variations is the relatively low accuracy of polarization measurements ($\sim 0.09\%$). Recently, Arora et al. (2019) conducted broadband polarimetric observations of DH Cep for only six nights, reporting that the average intrinsic linear polarization arising from DH Cep is less than 1%. These authors suggest that the degree and angle of the polarization appear to be dependent on the orbital phase.

In this paper, we present the results of our extensive high-precision polarimetric observational campaign, which was undertaken to probe phase-dependent variability in DH Cep. Moreover, in order to estimate the polarization in the vicinity of DH Cep, we measured the polarization from a sample of field stars identified as members of NGC 7380 and in close proximity to DH Cep. Our star selection is based on the findings of Mofat (1971), who conducted an extensive photometric study of 55 stars in the NGC 7380 cluster. We have chosen 14 stars from the list provided by this latter author, with distances similar to that of DH Cep. This not only gives us an estimate of interstellar polarization in the direction of DH Cep, but also helps us to understand the possible source of the observed polarization of DH Cep itself. Moreover, we explore the variation of the degree of polarization with the reddening of these stars in the cluster.

2. Polarimetric observations

DH Cep was observed over 42 nights, from 29 September until 29 December, 2017, with the DiPol-2 polarimeter (Piirola et al. 2014) installed on the remotely controlled T60 telescope at Haleakalā Observatory, Hawaii. The observational log is given in Table A.1.

DiPol-2 uses two dichroic beam-splitters to split the incident light beam into the B , V , and R passbands, which are simultaneously recorded by three CCD cameras. The polarimeter uses a superachromatic half-wave plate (HWP) as the polarization modulator and a plane-parallel calcite plate as the polarization analyzer. When observing bright stars such as DH Cep, DiPol-2 employs an intentional defocusing technique, which allows the collection of up to 10^7 photo-electrons per exposure, avoiding pixel saturation. For DH Cep, we acquired around 128 – 192 images every night with an exposure time of 5 – 7 s for each image, taken at different orientations of the HWP. This translates into 32 – 48 measurements of the Stokes q and u per night. We acquired a series of dark and bias images once per night. Skyflat images were obtained once per week, on average, in twilight hours, either at the beginning of the observing night or at dawn.

Our data reduction process involves a standard calibration algorithm with subtraction of bias and dark frames. Our polarimetry algorithm with DiPol-2 automatically eliminates flat-field effects over the areas exposed by the target images. We found that calibration with additional flat-field images does not considerably improve the results. After calibration, normalized Stokes q

and u parameters from the flux intensity ratios of the orthogonally polarized stellar images $Q_i = I_e(i)/I_o(i)$ are obtained for each orientation of the polarization modulator at $i = 0.0^\circ, 22.5^\circ, 45.0^\circ, 67.5^\circ$, and so on. The details of our data reduction procedure can be found in Piirola et al. (2020) and Abdul Qadir et al. (2023).

In order to determine the instrumental polarization, we observed 20 – 25 nonpolarized standard stars. The instrumental polarization in the B , V , and R bands was in the range of 0.004%–0.006% and the accuracy of the determination of instrumental polarization is 0.0002% – 0.0003%. To calibrate the polarization angle zero-point, we observed highly polarized standard stars HD 204827 and HD 25443 (see Table A.2 for their polarization degrees and angles). The resulting accuracy of the nightly average values of polarization measurements of DH Cep is at the level of 0.001% – 0.004% in the B and R bands and 0.002% – 0.006% in the V band.

3. Data analysis

3.1. Period search

To search for periodic signals in our polarimetric data, we employed a Lomb-Scargle algorithm (Lomb 1976; Scargle 1982). The benefit of using a Lomb-Scargle algorithm is that it uses the least squares method to fit a sinusoidal function to unevenly sampled data, which is often the case with astronomical data. To execute the Lomb-Scargle algorithm in PYTHON, we used the package from `astropy.timeseries`¹ (Price-Whelan et al. 2018).

The variations of the Stokes parameters of polarization arising from the scattered light in the binary system typically show two maxima and minima per orbital period separated by 0.5 in the orbital phase (Brown et al. 1978). Therefore, the Lomb-Scargle algorithm applied to polarization data is expected to detect half of the orbital period instead of the actual orbital period. We plotted the Lomb-Scargle periodograms for both Stokes q and u in the B , V , and R passbands in Figure 1. There are two clear, prominent peaks in each of these periodograms: at the frequencies of ~ 0.94 d⁻¹ and ~ 0.06 d⁻¹.

The first peak clearly indicates (half) the orbital period of DH Cep and the second peak is merely an alias of the first peak. An alias peak can appear when the frequency of the orbital period is not less than half of the sampling frequency, that is, the Nyquist frequency (f_{ny}). In such a situation, two waves are produced that differ by $1/f_{ny}$. The (half) orbital period for DH Cep, of namely ~ 1.055 d, is at a frequency of ~ 0.94 d⁻¹, which is more than half of the sampling frequency of ~ 0.47 d⁻¹, as we used data from 42 nights distributed over a period of about 90 d. Therefore, alias peaks can be expected at around $1/(1 - 1/1.055) = 19.18$ d or at frequency close to ~ 0.05 d⁻¹. As one can see, the alias peaks are quite close to that frequency in our periodograms (cf. Shannon (1949); VanderPlas (2018)). It is not uncommon to observe such alias peaks in Lomb-Scargle periodograms of astronomical data (e.g., Kosenkov & Veleđina (2018); Abdul Qadir et al. (2023)).

Furthermore, we calculated the false-alarm probability (FAP) for the (half) orbital period of DH Cep and its alias peaks (see Table 1) using a bootstrap method (Suveges 2012). The FAP values for both orbital peaks and alias peaks are very low, because the algorithm cannot distinguish between them. However, we conclude that the only period derived from our new polarization data corresponds to the known orbital period of 2.11 d. We

¹ <https://docs.astropy.org/en/stable/timeseries/lombscargle.html>

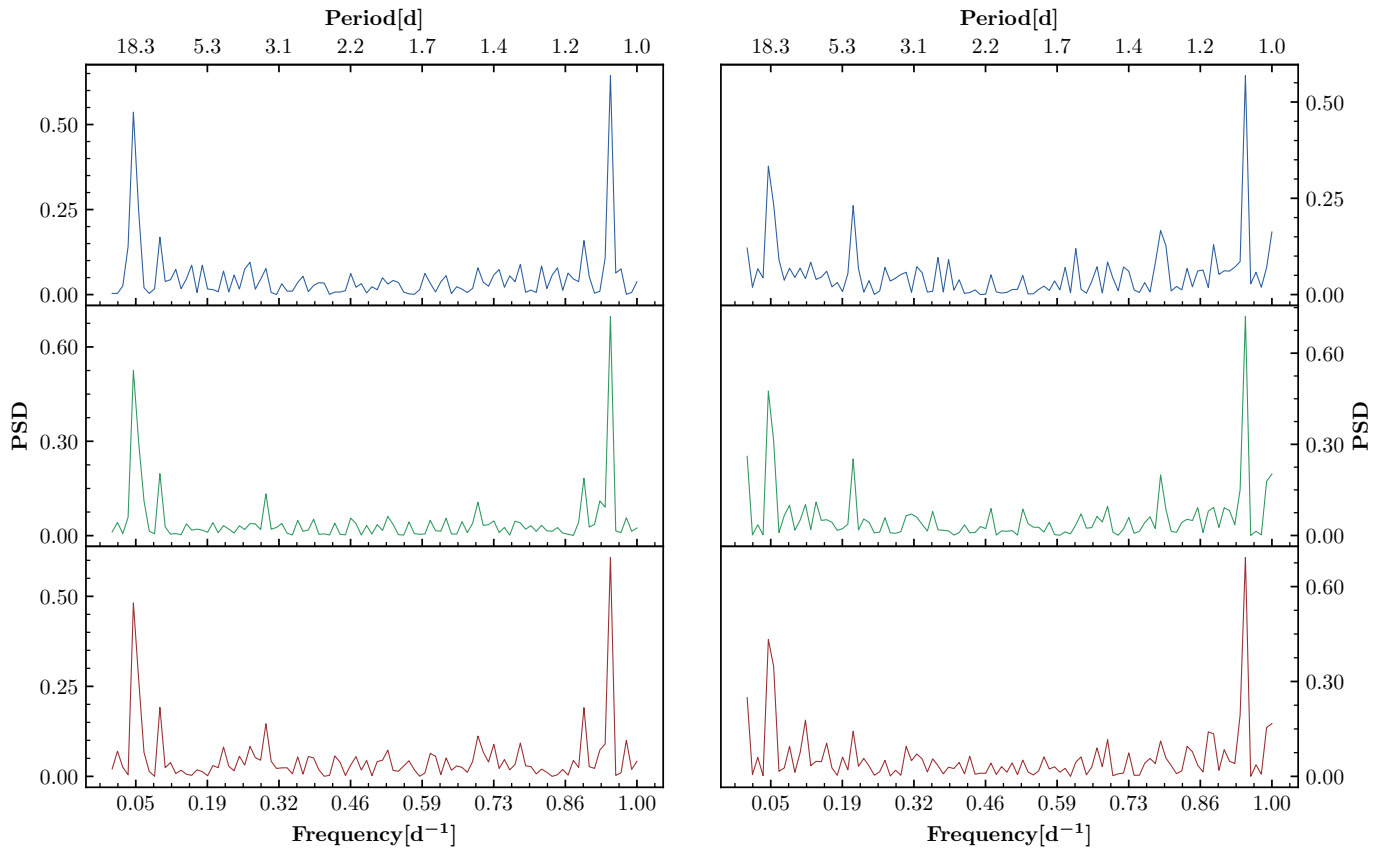


Fig. 1: Lomb-Scargle periodograms for Stokes q (left column) and u (right column) of DH Cep in B , V , and R passbands (top, middle and bottom panels respectively).

Table 1: FAP for DH Cep periodograms.

	Filter	Period[d]	FAP
Stokes q :	B	1.055	8.0×10^{-8}
		18.53	1.8×10^{-7}
	V	1.055	7.1×10^{-11}
		18.36	3.4×10^{-10}
R	1.055	5.4×10^{-8}	
	18.41	1.0×10^{-7}	
Stokes u :	B	1.055	9.1×10^{-10}
		18.35	9.0×10^{-9}
	V	1.055	4.7×10^{-13}
		18.46	3.4×10^{-13}
	R	1.055	1.7×10^{-11}
	18.41	5.6×10^{-11}	

do not detect the presence of any other (real) periodic signal in polarimetric data of DH Cep.

3.2. Interstellar polarization

DH Cep has a parallax of 0.3397 ± 0.0138 mas (Gaia Collaboration et al. 2021) and is a distant star located on the Galactic plane. Therefore, the observed polarization P_{obs} of DH Cep may contain a significant interstellar polarization component P_{is} due to a large amount of interstellar dust along the line of sight. In order to properly quantify P_{is} , we selected 14 field stars in the vicinity of DH Cep with parallaxes measured by the Gaia mission. All

these stars were previously identified as cluster members (Moffat 1971). Table 2 provides their SIMBAD² or Gaia DR3 identifiers (Gaia Collaboration et al. 2021)—with reference numbers that are the same as those given by Moffat (1971)—, coordinates, distances, parallaxes, reddening magnitudes, polarization degrees and angles, and the number of polarization measurements.

Figure 2 shows the dependence of the V-band polarization degree of the field stars and its angle on distance. We find that two stars from our sample, namely LS III +57 78 and LS III +57 82, have significantly larger parallaxes and are most likely foreground stars. In Figure 3, we depict these field stars together with their values of polarization and polarization angle on the coordinate plane (RA, Dec).

There is a noticeable scatter in the polarization degree (1.5% – 3.0%) in Figure 2, even within the narrow distance range of 2.6 – 3.3 kpc. The direction of polarization of the cluster stars shows only a moderate scatter (55° – 85°), with the average value being around 67° . For all measured stars, the polarization behavior with wavelength shows no peculiarities and is consistent with interstellar polarization. Due to the large scatter in the degree of polarization, using the average value of the polarization computed for all observed cluster stars as an estimate of the interstellar polarization component for DH Cep cannot be justified. However, we believe that the observed polarization values of star 21 can be used as a good first-order estimate. This star is very close to the binary in angular distance ($\sim 20''$) and its parallax and distance are the same as those of DH Cep within the errors of determination. Star 21 shows no apparent peculiarities

² <http://simbad.u-strasbg.fr/simbad/sim-fid>

Table 2: Identifiers, coordinates, parallaxes, distance, reddening magnitudes, polarization degrees, polarization angles, and the number of polarimetric observations of the field stars.

Identifier [SIMBAD/Gaia DR3]	Coordinates [J2000d]	Distance [kpc]	Parallax [mas]	E(B-V) [mag]	Filter	P [%]	θ [deg]	N_{obs}
LS III +57 83 (Ref 6)	341.8320563241, +58.1619232152	2.98	0.335 ±0.023	0.64	<i>B</i>	1.688±0.017	70.5 ± 0.3	16
					<i>V</i>	1.696±0.020	70.3 ± 0.3	16
					<i>R</i>	1.534±0.022	69.7 ± 0.4	16
LS III +57 90 (Ref 8)	341.9607907769, +58.0867661027	2.76	0.367±0.013	0.81	<i>B</i>	2.772±0.025	55.8 ± 0.3	16
					<i>V</i>	3.025±0.031	54.7 ± 0.3	16
					<i>R</i>	2.940±0.022	54.2 ± 0.2	16
LS III +57 86 (Ref 9)	341.9133361867, +58.1590438309	2.78	0.360±0.023	0.67	<i>B</i>	2.259±0.020	62.0 ± 0.3	16
					<i>V</i>	2.259±0.024	62.9 ± 0.3	16
					<i>R</i>	2.102±0.015	63.2 ± 0.2	16
LS III +57 81 (Ref 10)	341.8023077189, +58.1447839479	2.82	0.354±0.015	0.54	<i>B</i>	1.63±0.018	68.8 ± 0.3	16
					<i>V</i>	1.665±0.028	69.5 ± 0.5	16
					<i>R</i>	1.543±0.015	69.4 ± 0.3	16
LS III +57 78 (Ref 12)	341.7703133724, +58.1005319096	1.07	0.934±0.197	0.50	<i>B</i>	2.674±0.019	58.2 ± 0.2	16
					<i>V</i>	2.665±0.024	60.0 ± 0.3	16
					<i>R</i>	2.491±0.027	60.4 ± 0.3	16
LS III +57 84 (Ref 13)	341.8597287046, 58.2185710310	2.95	0.338±0.015	1.01	<i>B</i>	1.592±0.035	82.1 ± 0.6	16
					<i>V</i>	1.521±0.037	85.2 ± 0.7	16
					<i>R</i>	1.477±0.028	85.1 ± 0.5	16
LS III +57 89 (Ref 16)	341.9401580524, +58.1135622187	3.32	0.301±0.023	0.61	<i>B</i>	2.418±0.029	61.2 ± 0.3	16
					<i>V</i>	2.413±0.038	60.5 ± 0.4	16
					<i>R</i>	2.116±0.023	61.1 ± 0.3	16
LS III +57 85 (Ref 18)	341.8959575493, +58.1267941805	3.27	0.306±0.016	0.51	<i>B</i>	1.699±0.025	75.9 ± 0.4	16
					<i>V</i>	1.665±0.036	77.1 ± 0.6	16
					<i>R</i>	1.582±0.025	77.9 ± 0.5	16
LS III +57 79 (Ref 19)	341.7845019762, +58.0792187338	2.67	0.374±0.016	0.36	<i>B</i>	2.191±0.028	61.9 ± 0.4	16
					<i>V</i>	2.102±0.060	65.0 ± 0.8	16
					<i>R</i>	2.024±0.028	62.2 ± 0.4	16
2007416758659675136 (Ref 21)	341.7244663718, +58.0900466148	2.87	0.348±0.012	0.32	<i>B</i>	2.046±0.041	56.2 ± 0.6	96
					<i>V</i>	2.115±0.064	57.9 ± 0.9	96
					<i>R</i>	2.011±0.041	57.5 ± 0.6	96
LS III +57 82 (Ref 22)	341.8253457807, +58.1447160050	1.37	0.731±0.208	0.56	<i>B</i>	1.591±0.045	62.1 ± 0.8	15
					<i>V</i>	1.719±0.061	64.9 ± 1.0	15
					<i>R</i>	1.623±0.032	65.4 ± 0.6	15
2007422840333408256 (Ref 25)	341.7672786883, +58.1335887965	2.88	0.347±0.012	0.52	<i>B</i>	2.011±0.036	61.8 ± 0.5	16
					<i>V</i>	2.060±0.037	62.0 ± 0.5	16
					<i>R</i>	1.882±0.030	64.7 ± 0.5	16
LS III +57 87 (Ref 26)	341.9173203670, +58.1461523123	4.08	0.245±0.089	0.29	<i>B</i>	2.122±0.037	67.0 ± 0.5	16
					<i>V</i>	2.062±0.043	68.1 ± 0.6	16
					<i>R</i>	1.965±0.030	68.5 ± 0.4	16
LS III +57 80 (Ref 27)	341.7911729385, +58.1701205375	2.63	0.380±0.012	0.40	<i>B</i>	1.692±0.034	78.7 ± 0.6	16
					<i>V</i>	1.695±0.037	75.8 ± 0.6	16
					<i>R</i>	1.566±0.030	77.1 ± 0.5	16

and has no IR excess or emission lines. The direction of its polarization is close to the average direction of polarization in the cluster and its wavelength dependence is consistent with that of interstellar origin. Although we cannot exclude the presence of some intrinsic polarization in star 21, for a nonpeculiar single star to have intrinsic polarization of greater than a level of $\sim 10^{-4}$ is highly unlikely. Therefore, we adopt the polarization of star 21 as the best available approximation of interstellar polarization for DH Cep itself, keeping in mind the uncertainty due to the inhomogeneity of the interstellar polarization of the cluster member stars.

Table 3 provides the average observed polarization degree P_{obs} and angle θ_{obs} , the interstellar polarization degree P_{is} and angle θ_{is} computed for all cluster stars, and intrinsic polarization degree P_{int} and angle θ_{int} together with their errors for each pass-

band. The latter value is given with two pairs of columns: (a) derived with the average value of the observed polarization for all cluster stars, and (b) derived with the observed polarization of star 21 only. We note that values of P_{int} are very similar for both cases, while the values of θ_{int} differ by $\sim 20^\circ$.

The observed average value of polarization in DH Cep is relatively high ($\sim 2.5\%$), but after taking P_{is} into account, the value of the average intrinsic polarization P_{int} is reduced to $\sim 0.6\%$ with an average of $\theta_{\text{int}} \sim 83^\circ$. These values are similar to those derived by Corcoran (1991), but the estimation of $P_{\text{int}} \sim 1\%$ given by Arora et al. (2019) is somewhat higher than our value. The substantial value of P_{int} supports the conclusion made by Corcoran (1991) of the presence of a nonspherical circumstellar envelope in this binary system. However, in contrast to that reported by Corcoran (1991), we do not see a decrease in P_{obs} in

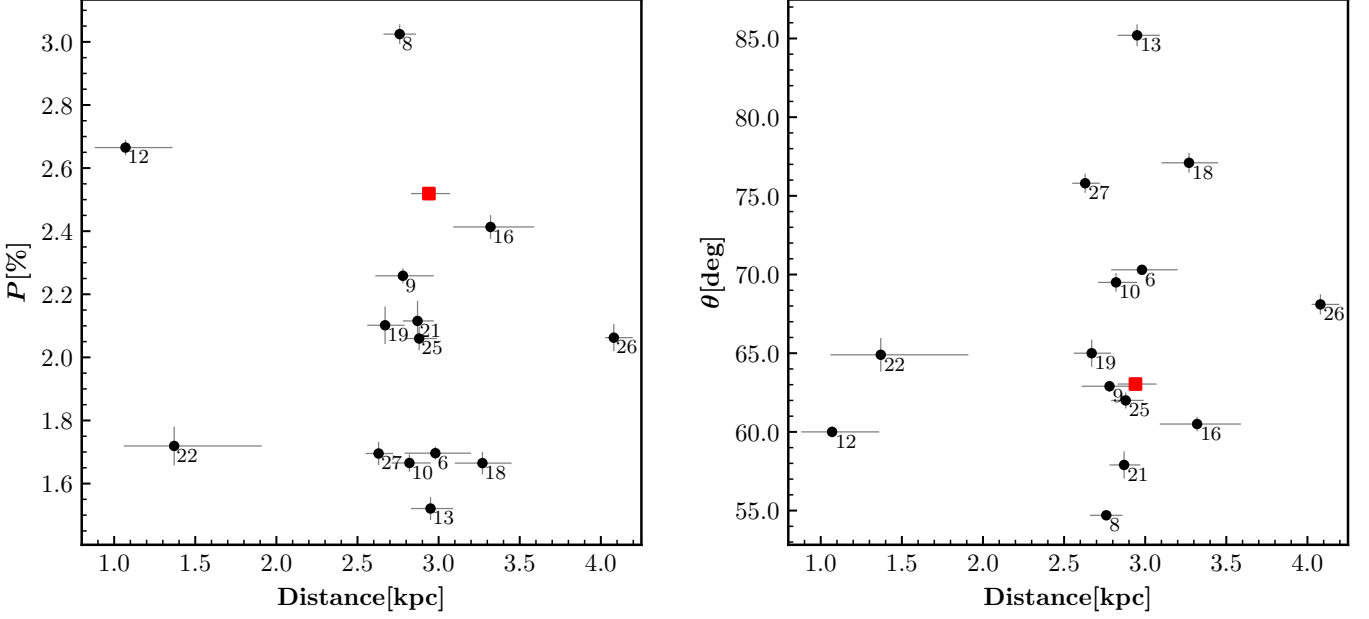


Fig. 2: Dependence of the observed degree of polarization P (left panel) and polarization angle θ (right panel) on distance in the V passband for DH Cep (red square) and field stars (black circles). Field stars are labeled as in Table 2. Error bars correspond to $\pm\sigma$ errors. The length of the error bar on distance for star 26 is divided by 20 for clarity.

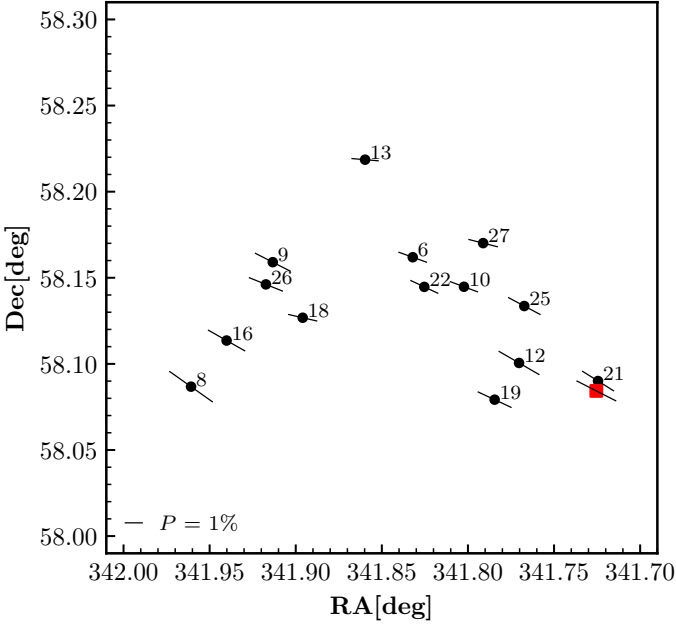


Fig. 3: Polarization map of DH Cep (red square) and field stars (black circles) in V passband. Bar length corresponds to the degree of linear polarization P , and the direction corresponds to the polarization angle (measured from the north to the east).

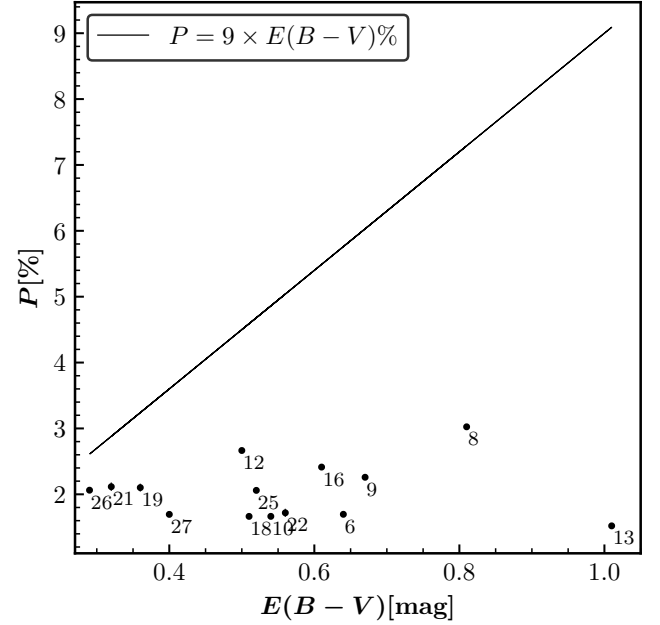


Fig. 4: Degree of polarization in the V band plotted versus reddening magnitude for each field star. The straight line in the plot corresponds to $P = 9 \times E(B - V)\%$. For most of the data points on this plot, the $\pm\sigma$ error bars are smaller than their plotting symbols. We note that stars 12 and 22 are foreground stars.

our polarimetric data, which were collected over the period of 90 days.

Figure 3 shows these field stars together with their values of polarization and polarization angles on the coordinate plane (RA, Dec). With regard to the interstellar polarization toward NGC 7380 cluster, a couple of attempts to measure this po-

larization were made in the distant past, providing values of $P_{is} = 1.3\% - 3.0\%$ and $\theta_{is} = 57^\circ - 83^\circ$ (Hoag (1953); McMillan (1976)). Our estimations are in good agreement with these older values. Moreover, when comparing polarization data ob-

Table 3: Average observed P_{obs} , θ_{obs} , average interstellar P_{is} , θ_{is} , and average intrinsic P_{int} , θ_{int} for DH Cep.

Filter	P_{obs} [%]	θ_{obs} [deg]	P_{is} [%]	θ_{is} [deg]	P_{int}^a [%]	θ_{int}^a [deg]	P_{int}^b [%]	θ_{int}^b [deg]
<i>B</i>	2.537 ± 0.001	61.5 ± 0.1	1.998 ± 0.029	66.7 ± 0.4	0.665 ± 0.029	51.8 ± 0.1	0.646 ± 0.029	79.2 ± 0.1
<i>V</i>	2.519 ± 0.001	63.0 ± 0.1	2.028 ± 0.038	67.2 ± 0.6	0.583 ± 0.038	56.2 ± 0.1	0.579 ± 0.038	83.4 ± 0.1
<i>R</i>	2.365 ± 0.001	63.5 ± 0.1	1.912 ± 0.026	67.6 ± 0.4	0.547 ± 0.026	57.0 ± 0.1	0.578 ± 0.026	86.7 ± 0.1

Notes. ^(a) The given values are derived using the average polarization of all observed field stars. ^(b) The given values are derived using the polarization of the field star 21.

tained for the same individual stars, our new measurements are in good agreement with those published by McMillan (1976).

Given the new set of polarization data for NGC 7380, we decided to study the dependence of the interstellar polarization in this cluster on reddening. For this purpose, we plotted the observed degree of linear polarization in the *V* band for our field stars against their reddening (Figure 4). For the reddenings, we used the values of $E(B - V)$ given by Moffat (1971). As is seen from the plot and in accordance with the conclusions made by McMillan (1976), the polarization of cluster stars most likely arises in the foreground dust layer, and the inter-cluster dust does not polarize. These conclusions are further supported by the fact that the two stars from our sample, LS III +57 78 and LS III +57 82, have significantly larger parallaxes; they are most likely foreground stars, but still show similar polarization degrees and angles to other stars in our sample of field stars. For this reason, there is no apparent increase in P with the increase in $E(B - V)$ (see Figure 4). We can also see that the polarization of every field star follows the empirical interstellar medium polarization law: $P \leq 9 \times E(B - V)\%$ (Serkowski et al. 1975).

3.3. Polarization variability

We used a standard analytical method based on a two-harmonic Fourier fit (commonly known as the Brown McLean Emslie (BME) approach (Brown et al. 1978)) to fit the phase-folded curves of the Stokes q and u parameters. This method assumes a circular orbit with a co-rotating light-scattering envelope and the fit includes zeroth, first, and second harmonics terms:

$$\begin{aligned} q &= q_0 + q_1 \cos \lambda + q_2 \sin \lambda + q_3 \cos 2\lambda + q_4 \sin 2\lambda, \\ u &= u_0 + u_1 \cos \lambda + q_2 \sin \lambda + q_3 \cos 2\lambda + q_4 \sin 2\lambda, \end{aligned} \quad (1)$$

where $\lambda = 2\pi\phi$ and ϕ is a phase of the orbital period. The polarimetric data of Stokes q and u were phase folded using the orbital period: P_{orb} [d] = 2.11095, and ephemeris: T_0 [MJD] = 2456525.564 (Martins et al. 2017), which refers to the time of the conjunction (primary in front). We employed the `curve_fit` function of the `scipy.optimize`³ library in PYTHON to obtain best-fit coefficients together with their errors, as shown in Table 4. With these coefficients, we performed the curve fitting of the observed polarization data (plots are shown in Figure 5).

As is seen from the fit, the amplitude of the variability is $\sim 0.2\%$ with noticeable nonperiodic scatter, which is most pronounced in the Stokes q and in the B-band. Revealing such small-amplitude periodic variability with confidence requires precision at the level of $\leq 0.03\%$. It appears that the main reason for the nondetection of phase-dependent polarization variability in DH Cep by Corcoran (1991) was the relatively low accuracy

³ <https://docs.scipy.org/doc/scipy/reference/optimize.html>

of polarization measurements. The much higher accuracy that we achieve here allows us to reveal clear periodic variations, showing that nonperiodic scatter of polarization is real; that is, it does not arise from measurement errors.

One can deduce the orbital inclination i using the values of the first ($q_{1,2}$, $u_{1,2}$) and second ($q_{3,4}$, $u_{3,4}$) harmonics terms of Fourier series with equations given by Drissen et al. (1986) (see Appendix B). However, for a circular orbit and distribution of the light scattering material symmetric to the orbital plane, first harmonics terms are negligibly small, and therefore only second harmonics terms can be used in practice. This is clearly the case for DH Cep. In addition to the orbital inclination, the orientation of the orbit on the sky (longitude of ascending node Ω) can be determined (see Appendix B).

A_q and A_u are the two parameters that define the ratio of the amplitudes of the second and first harmonics for Stokes q and u , respectively. These parameters are effective measures of the degree of symmetry and the concentration of scattering material towards the orbital plane in a circular orbit. Formulae for deriving these parameters are also given in Appendix B.

Using Eqs. (B1 – B4), we derived the values of i , Ω , A_q , and A_u for the *B*, *V*, and *R* passbands, which are given in Table 5. We can definitely say that second harmonics terms are dominant for both Stokes q and u parameters in all three passbands. There are small but apparently nonzero first harmonics in the variability of Stokes q and u seen in the *V* and *R* bands, but not to the extent that would explicitly confirm a significant asymmetry of light-scattering material, which was suggested by Corcoran (1991).

It is well known that due to the noise in polarimetric data arising from measurement uncertainties, the derived values of i from the Fourier fit are always biased towards higher values (Aspin et al. (1981); Simmons et al. (1982); Wolinski & Dolan (1994)). The amount of bias depends on the value of true inclination; the lower the true value of i , the greater the bias toward higher values. A similar bias toward higher values can be induced by the stochastic noise caused by the intrinsic nonperiodic component of polarimetric variations (Manset & Bastien 2000). This bias also affects 1σ and 2σ confidence intervals, which become asymmetric, with the lower border extending toward smaller values of i . In the case of small i and γ (Eq. 2) values, the lower boundary of the confidence interval may extend to $i = 0^\circ$. If this happens, polarimetry may only provide an upper limit on the true value of inclination. Moreover, the width of Ω confidence interval(s) increases rapidly with decreasing inclination (Wolinski & Dolan 1994).

Figure 5 reveals significant scatter around the fitting curves in all passbands. The fit for the *B* passband—particularly for the Stokes q —is the most affected. The value of the standard deviation σ for the B-band q fit is ≈ 0.06 , which is about twice those for the *V*- and *R*-band fits. We emphasize that nonperiodic noise is not due to observational errors, which are smaller than $\leq 0.005\%$ for all wavelength bands. The presence of real

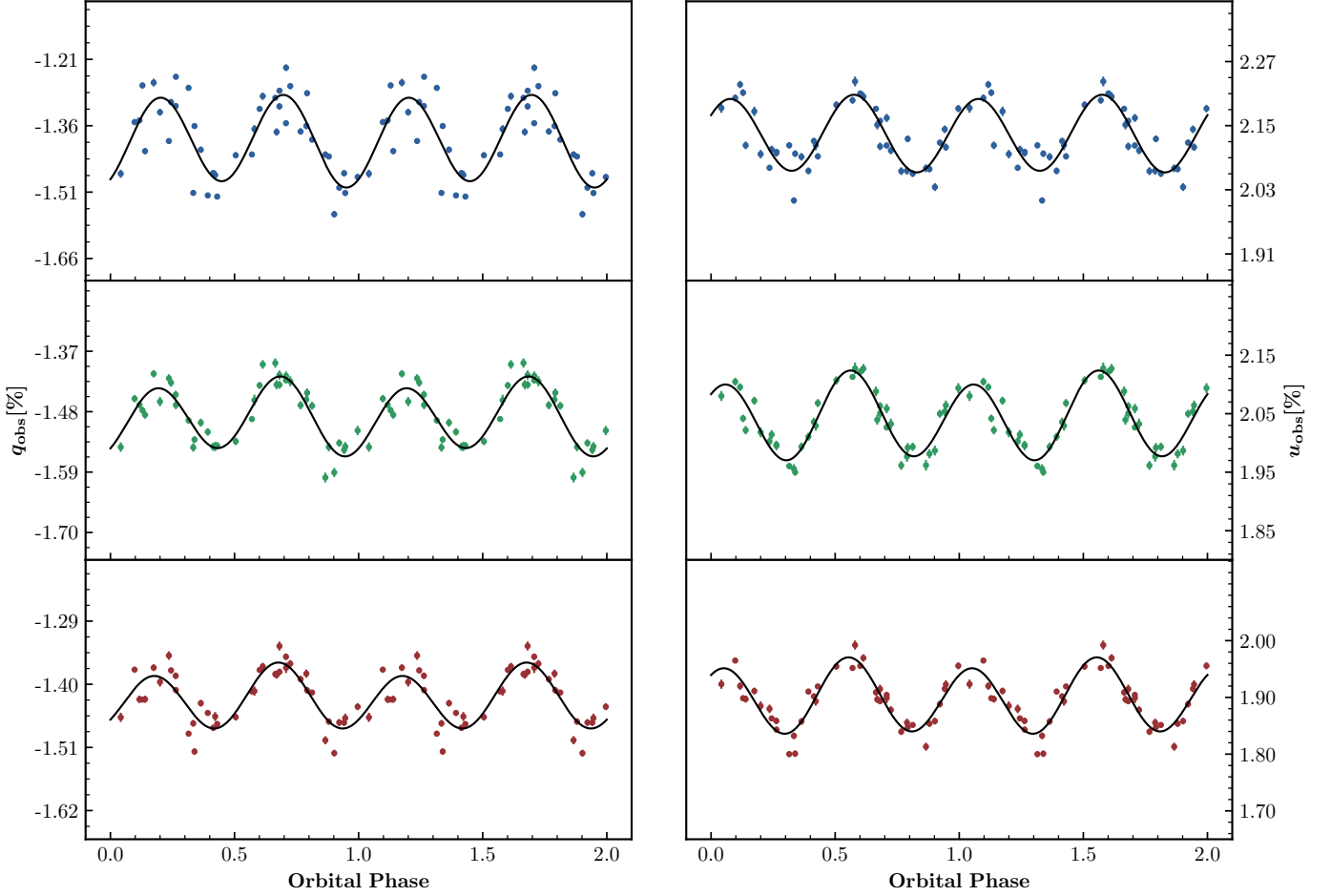


Fig. 5: Variability of observed Stokes parameters q and u for DH Cep in B , V , and R passbands (top, middle, and bottom panels respectively) phase-folded with the orbital period of 2.11 d. Fourier fit curves (see Sect. 3.3) are shown with solid lines, and the best-fit Fourier coefficients are given in Table 4. The error bars correspond to $\pm\sigma$ errors.

Table 4: Fourier coefficients for Stokes q and u .

Filter	q_0	q_1	q_2	q_3	q_4	u_0	u_1	u_2	u_3	u_4
B	-1.3924	-0.0078	-0.0008	-0.0801	0.0590	2.1337	-0.0042	-0.0005	0.0399	0.0575
	± 0.0086	± 0.0129	± 0.0109	± 0.0129	± 0.0113	± 0.0046	± 0.0070	± 0.0059	± 0.0070	± 0.0061
V	-1.4911	-0.0110	-0.0071	-0.0456	0.0442	2.0432	-0.0098	-0.0075	0.0503	0.0471
	± 0.0037	± 0.0055	± 0.0048	± 0.0056	± 0.0048	± 0.0032	± 0.0047	± 0.0041	± 0.0048	± 0.0041
R	-1.4290	-0.0052	-0.0105	-0.0312	0.0410	1.8958	-0.0084	-0.0051	0.0484	0.03787
	± 0.0041	± 0.0060	± 0.0053	± 0.0062	± 0.0053	± 0.0032	± 0.0047	± 0.0041	± 0.0048	± 0.0041

stochastic variability in DH Cep polarization is relatively clear. The natural explanation for this phenomenon is highly clumped radiatively driven stellar wind, which is not uncommon in early-type binaries such as DH Cep (a discussion on the polarization mechanism is presented in Section 4).

As expected, because of the larger amplitude of the noise, the inclination derived for the B-band will be the most affected; that is, it will be shifted toward higher values by the bias. As DH Cep is not an eclipsing binary, the true inclination should be rather small. As mentioned in the previous paragraph, a true lower inclination causes greater bias and more asymmetric confidence interval(s) for derived inclination i , and widens the confidence intervals for Ω . In order to quantify this bias, we derived confidence intervals for i and Ω using the method proposed by Wolinski & Dolan (1994). This method uses the special merit

parameter γ , which is defined as

$$\gamma = \left(\frac{A}{\sigma_p} \right)^2 \frac{N}{2}, \quad (2)$$

where A is the fraction of the amplitude of polarization variability, defined as:

$$A = \frac{|q_{\max} - q_{\min}| + |u_{\max} - u_{\min}|}{4}, \quad (3)$$

where σ_p is a standard deviation that is determined from the scatter of the observed Stokes parameters around the best-fit curves, N is the number of observations, and q_{\max} , q_{\min} , u_{\max} , u_{\min} are the maximum and minimum values of the fitted curve of Stokes parameters q and u . Our derived values of σ_p are 0.055, 0.030,

Table 5: Orbital Parameters of DH Cep in B , V , and R passbands. The parameters A_q and A_u are defined in Eq. B.4.

Filter	i^a	i^b	Ω	A_q/A_u
B	66°	64°	$2^\circ(182^\circ)$	16.7/12.7
V	50°	46°	$105^\circ(285^\circ)$	4.1/5.6
R	57°	55°	$88^\circ(268^\circ)$	4.4/6.8

Notes. ^(a) The given values are derived using best-fit Fourier coefficients. ^(b) The given values are de-biased.

and 0.031 and those of γ are 65, 158, and 93 for the B , V , and R bands, respectively.

To estimate the bias and confidence intervals for i and Ω , we used the plots given in (Wolinski & Dolan (1994); Figs. 4 and 6(c) therein, where $\gamma = 75.0$, which is closest to our obtained γ values). The resulting de-biased values for i are 64° , 46° , and 55° in the B , V and R passbands, respectively. The corresponding lower limits on the 1σ confidence interval for i extend to 0° for all passbands, whereas the upper limits are 67° , 57° , and 61° . Similarly, the values for Ω with a 1σ confidence interval are $2^\circ(182^\circ) \pm 55^\circ$, $105^\circ(285^\circ) \pm 55^\circ$, and $88^\circ(268^\circ) \pm 55^\circ$ for the B , V , and R bands. It is to be noted that there is ambiguity as to the value of Ω , as $\Omega + 180^\circ$ is equally possible (Drissen et al. 1986).

Furthermore, we show the ellipses of the second harmonics on the (q, u) plane in Figure 6, which also shows average interstellar polarization for the B , V , and R bands. The eccentricity of the ellipses is related to the inclination of the orbit i , and the orientation of their major semi-axes with respect to the q -axis defines the orientation of the orbit Ω . The direction of circumvention corresponds to the direction of the orbital motion in the binary system on the plane of the sky. As one can see, the ellipse for the B-band is oriented almost perpendicular to those for the V and R bands. We believe that this is most likely an effect of the nonperiodic noise on the Fourier fit, which introduces a large uncertainty on the orientation of the second harmonics ellipses on the (q, u) plane. Due to the fact that the derived value of inclination is: $90^\circ \leq i \leq 180^\circ$, the binary system rotation on the plane of the sky is clockwise. The values given in Table 5 are subtracted from 180° .

The very first estimation of $i = 62^\circ$ was given by Pearce (1949) from the analysis of spectroscopic observations. However, such a large inclination value would likely allow eclipses of the two components and this estimate was later rejected. From their photometric observations, Lines et al. (1986) estimated the inclination to be between 45° and 55° . Based on their estimation, Corcoran (1991) adopted a value of 50° . Later on, the photometric observations of Lines et al. (1986) were modeled by Sturm & Simon (1994) and Hilditch et al. (1996) and both derived $i = 47^\circ \pm 1^\circ$, which has since been accepted as the inclination value of the orbit of DH Cep. Our de-biased value of $i = 46^\circ$ in the V band, which is our best estimate among three passbands, is very similar to that value. However, our derived value is slightly higher than the upper limit of $i = 43^\circ$ provided by Penny et al. (1997).

4. Discussion

The analytical solution of BME does not take into account the finite size of the stars or the eclipses of the scattering material that may take place in close-binary systems. Moreover, this method does not provide detailed information on the distribution of the scattering material that is responsible for the observed po-

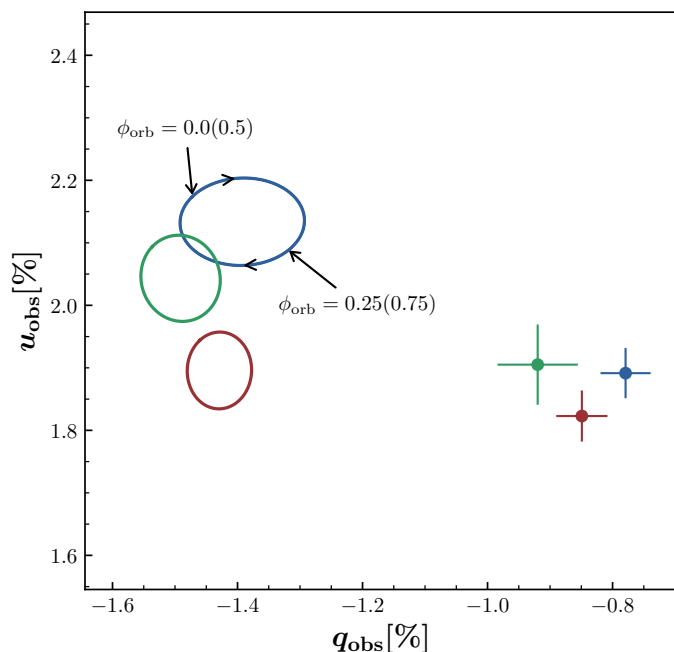


Fig. 6: Variability of observed polarization for DH Cep plotted on the Stokes (q, u) plane, represented by the ellipses of the second harmonics of the Fourier fit. Blue, green, and red colors represent the B , V , and R passbands, respectively. The clockwise direction and phases of the orbital period are depicted for the B band ellipse. The angle between the major axis and the q -axis gives the orientation Ω . Average interstellar (Ref 21) Stokes q and u parameters are depicted as circles with $\pm\sigma$ error bars.

larization variability. Numerical modeling can be employed that takes into account the finite sizes of the components, the distance between them, and the various scattering scenarios that are the most relevant for a given system. As DH Cep is an O-type binary, the most likely cause of the polarization variations is electron scattering in the stellar winds of the hot components. In their study of the stars of the NGC 7380 cluster, Massey et al. (1995) re-classified the components of the DH Cep binary and added ((f)) to their spectral types, which suggests significant stellar winds. The analysis of the short-wavelength prime (SWP) spectrum of DH Cep provided by the IUE, which is accessible through the MAST⁴ archive, reveals the unambiguous presence of a strong C iv $\lambda 1550$ wind profile, which indicates that either one or both of the stars exhibit strong wind (Corcoran 1991). Another possible mechanism is the reflection of light off the facing hemisphere of the components; see for example the case of the O-type binary system LZ Cep (Berdyugin & Harris 1999). However, we defer a detailed modeling to our upcoming paper, in which we will perform a numerical modeling of the periodic polarization variability in the early-type systems AO Cas, DH Cep, and HD 165052 in the same way as was already done for the O-type system HD 48099 (Berdyugin et al. 2016).

The polarization variability amplitudes computed from our fit to the data are 0.085, 0.063, and 0.052 %, in the B , V , and R passbands, respectively. The scatter due to the nonperiodic component, as determined from the standard deviation, is also larger in the B band. As electron scattering is gray, all amplitudes should be equal irrespective of wavelength. The observed difference in the amplitude may be attributable to the dilution

⁴ <https://archive.stsci.edu/index.html>

of unpolarized radiation from a larger volume around the binary system, which in turn is due to the increasing amount of free-free continuum emission toward the red. We note that this dilution has the same effect on both periodic and nonperiodic polarization components, explaining the smaller scatter in the V and R passbands.

Moreover, we deduced the mass-loss rate using the model given by St.-Louis et al. (1988). This method employs the amplitude (A_p) of the linear polarimetric variability:

$$A_p = \frac{(1 + \cos^2 i) 3\sigma_t f_c \dot{M}}{(16\pi)^2 m_p v_\infty a} I, \quad (4)$$

where \dot{M} is mass-loss rate, f_c is the fraction of the total light coming from the companion star, v_∞ is the terminal velocity of the wind, a is semi-major axis, and I is an integral:

$$I = \int_0^\infty \int_0^\pi \int_0^{2\pi} \frac{\sin^3 \theta \cos 2\phi d(R/a) d\theta d\phi}{(R'/a)^2 (1 - R_*/R')^\beta}. \quad (5)$$

We note that primed coordinates are measured relative to the primary star, while unprimed coordinates originate at the secondary star. In order to evaluate this integral, one has to choose a specific wind velocity law: $v(R') = v_\infty (1 - R_*/R')^\beta$, which is characterized by the parameter β . We can rewrite Eq. 4 as follows:

$$\dot{M} = \frac{(16\pi)^2 m_p v_\infty a A_p}{(1 + \cos^2 i) 3\sigma_t f_c I},$$

or

$$\dot{M}[M_\odot \text{ yr}^{-1}] = \frac{2.33 \times 10^{-7} v_\infty (\text{km s}^{-1}) a (R_\odot) A_p}{(1 + \cos^2 i) f_c I}. \quad (6)$$

Using our results for polarimetric variations in V passband, we obtain $A_p = 0.00063$ (we note that the value of A is given earlier in this section as a percentage), and $i = 46^\circ$. Corcoran (1991) gave the terminal wind velocity of the primary as $v_\infty = 3000 \text{ km s}^{-1}$. The semi-major axis $a = 6.8 R_\odot$ (Penny et al. 1997), while $f_c = (1 + 10^{-0.4\Delta M_v})^{-1} = 0.475$, for which we used $M_v = -4.66$ and $M_v = -4.55$ (Hilditch et al. 1996) for the primary and the secondary components, respectively. We used the plot given by (St.-Louis et al. (1988); Fig. 9 therein) in order to choose the appropriate value of $I = 12.5$, which is obtained for $\beta = 0.8$ as suggested by Abbott et al. (1986) and Corcoran (1991) for O-type stars, $\epsilon = R'_i/R_* = 1.0$ (assuming that the scattering envelope is optically thin), where R'_i is measured with respect to the center of the primary star, and $a/R_* \sim 1$ using the value of $R_* = 8.1 R_\odot$ for $i = 47^\circ$ given by Penny et al. (1997). These values yield $\dot{M} = 1.7 \times 10^{-7} M_\odot \text{ yr}^{-1}$ (the value of A_p is divided by two as we assume two equal winds in O+O binaries (St-Louis & Moffat 2008)) for the primary component of DH Cep, and \dot{M} for the binary system would be about twice this value, which is lower than the mass-loss rate of $\sim 2 \times 10^{-6} M_\odot \text{ yr}^{-1}$ estimated by Corcoran (1991).

5. Conclusions

We conducted the first comprehensive high-precision polarimetric study of the O+O-type binary DH Cep. This study reveals clear periodically variable linear polarization with an amplitude of $\sim 0.2\%$. The periodic signal frequency, which corresponds to

half of the previously determined orbital period of 2.11 d, was found using the Lomb-Scargle algorithm. In addition to periodic variability, there are significant nonperiodic fluctuations of the intrinsic polarization. The nonperiodic variability component effectively limits the accuracy of estimates of orbital parameters that can be derived from the Fourier fit to polarization data. Furthermore, our study allows us to obtain an estimate of the interstellar polarization component in DH Cep based on the observed polarization of the closely located field star 21. If this estimate is accurate, most of the DH Cep polarization ($\sim 2.0\%$) is of interstellar nature, and this binary system exhibits a $\sim 0.6\%$ intrinsic polarization component. This supports the presence of a non-spherical circumstellar scattering envelope in DH Cep system, which was previously suggested by Corcoran (1991). However, we do not detect any decrease in the degree of observed polarization on a timescale of three months, which is in contrast to the findings of these latter authors.

We find that for the DH Cep system, the second harmonics of the orbital period clearly dominate the observed periodic variability, which suggests a nearly symmetric geometry of the light scattering material with respect to the orbital plane. The orbital parameters derived from our best (smoothest) Fourier fit to the V -band data are: $i = 46^\circ + 11^\circ / -46^\circ$ and $\Omega = 105^\circ \pm 55^\circ$. Our derived orbital inclination value is in good agreement with the most commonly adopted value of $47^\circ \pm 1^\circ$. Using this value, together with the polarimetric amplitude in the V passband, we estimate the mass-loss rate in the binary system to be $\sim 3.4 \times 10^{-7} M_\odot \text{ yr}^{-1}$. The direction of motion on the orbit, as seen on the sky, is clockwise.

This study is part of a series of investigations of linear polarization arising from O-type binary systems. We have already published our studies of HD 48099 (Berdyugin et al. 2016) and AO Cas (Abdul Qadir et al. 2023) and are presently studying HD 165052. In a future paper of this series, we will present the results of our numerical scattering code modeling for DH Cep along with AO Cas and HD 165052 systems. This modeling will help to put constraints on the distribution of light-scattering material in these O-type binaries.

Acknowledgements. This work was supported by the ERC Advanced Grant HotMol ERC-2011-AdG-291659 (www.hotmol.eu). Dipol-2 was built in the cooperation between the University of Turku, Finland, and the Kiepenheuer Institut für Sonnenphysik, Germany, with the support by the Leibniz Association grant SAW-2011-KIS-7. We are grateful to the Institute for Astronomy, University of Hawaii for the observing time allocated for us on the T60 telescope at the Haleakalā Observatory. We are thankful to Vadim Kravtsov for helpful discussions regarding confidence intervals on derived values of orbital parameters. All raw data and calibrations images are available on request from the authors.

References

- Abbott, D. C., Beiging, J. H., Churchwell, E., & Torres, A. V. 1986, *ApJ*, 303, 239
- Abdul Qadir, Y., Berdyugin, A. V., Piirola, V., Sakanoi, T., & Kagitani, M. 2023, *A&A*, 670, A176
- Arora, B., Pandey, J. C., Joshi, A., & De Becker, M. 2019, *Bulletin de la Societe Royale des Sciences de Liege*, 88, 287
- Aspin, C., Simmons, J. F. L., & Brown, J. C. 1981, *MNRAS*, 194, 283
- Berdyugin, A., Piirola, V., Sadegi, S., et al. 2016, *A&A*, 591, A92
- Berdyugin, A. V. & Harris, T. J. 1999, *A&A*, 352, 177
- Bhatt, H., Pandey, J. C., Kumar, B., Sagar, R., & Singh, K. P. 2010, *New A*, 15, 755
- Brown, J. C., McLean, I. S., & Emslie, A. G. 1978, *A&A*, 68, 415
- Corcoran, M. F. 1991, *ApJ*, 366, 308
- Drissen, L., Lamontagne, R., Moffat, A. F. J., Bastien, P., & Seguin, M. 1986, *ApJ*, 304, 188
- Gaia Collaboration, Brown, A. G. A., Vallenari, A., et al. 2021, *A&A*, 649, A1
- Hilditch, R. W., Harries, T. J., & Bell, S. A. 1996, *A&A*, 314, 165

- Hoag, A. A. 1953, *AJ*, 58, 42
- Kosenkov, I. A. & Veledina, A. 2018, *MNRAS*, 478, 4710
- Lata, S., Pandey, A. K., Panwar, N., et al. 2016, *MNRAS*, 456, 2505
- Lines, H. C., Lines, R. D., Guinan, E. F., & Robinson, C. R. 1986, *Information Bulletin on Variable Stars*, 2932, 1
- Lomb, N. R. 1976, *Ap&SS*, 39, 447
- Manset, N. & Bastien, P. 2000, *AJ*, 120, 413
- Martins, F., Mahy, L., & Hervé, A. 2017, *A&A*, 607, A82
- Massey, P., Johnson, K. E., & Degioia-Eastwood, K. 1995, *ApJ*, 454, 151
- McMillan, R. S. 1976, *AJ*, 81, 970
- Moffat, A. F. J. 1971, *A&A*, 13, 30
- Pearce, J. A. 1949, *AJ*, 54, 135
- Penny, L. R., Gies, D. R., & Bagnuolo, William G., J. 1997, *ApJ*, 483, 439
- Piirola, V., Berdyugin, A., & Berdyugina, S. 2014, in *Society of Photo-Optical Instrumentation Engineers (SPIE) Conference Series*, Vol. 9147, *Ground-based and Airborne Instrumentation for Astronomy V*, ed. S. K. Ramsay, I. S. McLean, & H. Takami, 914781
- Piirola, V., Berdyugin, A., Frisch, P. C., et al. 2020, *A&A*, 635, A46
- Piirola, V., Kosenkov, I. A., Berdyugin, A. V., Berdyugina, S. V., & Poutanen, J. 2021, *AJ*, 161, 20
- Price-Whelan, A., Crawford, S., Sipocz, B., et al. 2018, *Astropy/Astropy-V2.0-Paper: Final Draft*, Zenodo
- Scargle, J. D. 1982, *ApJ*, 263, 835
- Schmidt, G. D., Elston, R., & Lupie, O. L. 1992, *AJ*, 104, 1563
- Serkowski, K., Mathewson, D. S., & Ford, V. L. 1975, *ApJ*, 196, 261
- Shannon, C. E. 1949, *IEEE Proceedings*, 37, 10
- Simmons, J. F. L., Aspin, C., & Brown, J. C. 1982, *MNRAS*, 198, 45
- St.-Louis, N., Moffat, A. F. J., Drissen, L., Bastien, P., & Robert, C. 1988, *ApJ*, 330, 286
- St-Louis, N. & Moffat, A. F. J. 2008, in *Clumping in Hot-Star Winds*, ed. W.-R. Hamann, A. Feldmeier, & L. M. Oskinova, 39
- Sturm, E. & Simon, K. P. 1994, *A&A*, 282, 93
- Suveges, M. 2012, in *Seventh Conference on Astronomical Data Analysis*, ed. J.-L. Starck & C. Surace, 16
- Underhill, A. B. 1969, *A&A*, 1, 356
- VanderPlas, J. T. 2018, *ApJS*, 236, 16
- Wolinski, K. G. & Dolan, J. F. 1994, *MNRAS*, 267, 5
- Wu, C. C. & Eaton, J. A. 1981, *Information Bulletin on Variable Stars*, 1965, 1

Appendix A: Tables

Table A.1: Log of polarimetric observations for DH Cep.

Date	MJD	$T_{\text{exp}}[\text{s}]$	N_{obs}
2017-09-29	58025.87	800	40
2017-09-30	58026.87	640	32
2017-10-01	58027.89	640	32
2017-10-03	58029.86	640	32
2017-10-05	58031.90	800	40
2017-10-06	58032.87	800	40
2017-10-07	58033.85	800	40
2017-10-08	58034.88	800	40
2017-10-10	58036.80	800	40
2017-10-11	58037.89	800	40
2017-10-18	58044.83	800	40
2017-10-19	58045.82	1600	40
2017-10-21	58047.82	1560	39
2017-10-22	58048.83	1600	40
2017-10-27	58053.78	800	40
2017-10-28	58054.80	1600	40
2017-11-02	58059.78	800	40
2017-11-03	58060.78	1120	40
2017-11-05	58062.85	1792	64
2017-11-06	58063.75	800	40
2017-11-07	58064.74	880	44
2017-11-09	58066.76	1344	48
2017-11-10	58067.76	1344	48
2017-11-15	58072.77	1148	41
2017-11-16	58073.76	1344	48
2017-11-17	58074.75	1344	48
2017-11-18	58075.77	1120	40
2017-11-20	58077.78	1344	48
2017-11-21	58078.78	1120	40
2017-11-22	58079.78	1120	40
2017-11-25	58082.77	1120	40
2017-12-04	58091.72	1344	48
2017-12-05	58092.72	1344	48
2017-12-06	58093.72	1288	46
2017-12-07	58094.71	1344	48
2017-12-08	58095.71	1344	48
2017-12-11	58098.72	1344	48
2017-12-12	58099.71	1568	56
2017-12-14	58101.73	1120	40
2017-12-15	58102.72	1344	48
2017-12-26	58113.70	1344	48
2017-12-29	58116.73	1120	40

 Table A.2: Average polarization degrees (P), and polarization angles (θ) of highly polarized stars.

Star	Filter	P [%]	θ [deg]	Ref.
HD 204827	B	5.789 ± 0.011	57.79 ± 0.02	[1]
	V	5.602 ± 0.019	58.33 ± 0.02	[1]
	R	5.079 ± 0.011	59.21 ± 0.02	[1]
HD 25443	B	5.232 ± 0.092	134.28 ± 0.51	[2]
	V	5.127 ± 0.061	134.2 ± 0.34	[2]
	R	4.734 ± 0.045	133.65 ± 0.28	[2]

References. (1) Piirola et al. (2021); (2) Schmidt et al. (1992).

Appendix B: Formulae

The formulae given by Drissen et al. (1986) are given in this section. For the orbital inclination (i):

$$\begin{aligned} \left(\frac{1 - \cos i}{1 + \cos i} \right)^4 &= \frac{(u_1 + q_2)^2 + (u_2 - q_1)^2}{(u_2 + q_1)^2 + (u_1 - q_2)^2} \\ &= \frac{(u_3 + q_4)^2 + (u_4 - q_3)^2}{(u_4 + q_3)^2 + (u_3 - q_4)^2}. \end{aligned} \quad (\text{B.1})$$

The longitude of the ascending node (Ω) can be computed using the following:

$$\tan \Omega = \frac{A + B}{C + D} = \frac{C - D}{A - B}, \quad (\text{B.2})$$

where,

$$\begin{aligned} A &= \frac{u_4 - q_3}{(1 - \cos i)^2}, & B &= \frac{u_4 + q_3}{(1 + \cos i)^2}, \\ C &= \frac{q_4 - u_3}{(1 + \cos i)^2}, & D &= \frac{u_3 + q_4}{(1 - \cos i)^2}. \end{aligned} \quad (\text{B.3})$$

The following formulae can be used to derive A_q and A_u :

$$A_q = \sqrt{\frac{q_3^2 + q_4^2}{q_1^2 + q_2^2}}, \quad A_u = \sqrt{\frac{u_3^2 + u_4^2}{u_1^2 + u_2^2}}. \quad (\text{B.4})$$